Biomimetic Intelligence and Robotics 3 (2023) 100128

Contents lists available at ScienceDirect

Biomimetic Intelligence and Robotics

journal homepage: www.elsevier.com/locate/birob

Research Article

Visual servoing-based pneumatic hair transplantation mechanism for robotic FUE surgery

Fulin Jia, Shenghao Yang, Chenxi Han, Junye Li, Xuanru Han, Chao Zhang, Jiaole Wang *,1

School of Mechanical Engineering and Automation, Harbin Institute of Technology (Shenzhen), Shenzhen 518055, China

ARTICLE INFO

Article history:
Received 30 August 2023
Revised 3 October 2023
Accepted 8 October 2023
Available online 10 October 2023

Keywords:
Robotic hair transplantation
Follicle unit extraction (FUE)
Image-based visual servoing (IBVS)

ABSTRACT

Hair transplantation surgery is an effective solution for hair loss problems, among which follicle unit extraction (FUE) surgery is more widely used and favored. At present, most hair transplantation surgeries still rely heavily on manual operation by doctors and very few hair transplantation robots with complex structures have been introduced. This paper proposes a pneumatic hair transplantation mechanism for FUE surgery, equipped with a camera, capable of automatically performing both hair implantation and extraction with airflow. This pneumatic method eliminates the complex needle structure, has the function of temporarily storing the follicles inside the needle, thus facilitating the automation of transferring follicles from extraction to implantation. Then a visual feedback system is proposed to accurately position the follicles during the transplantation. The experimental results show that average distance deviation between the actual and target positions is 0.6128 mm and the average deviation of hair implantation depth is 1.7176 mm, which verify the feasibility of the proposed system.

1. Introduction

1.1. Background

Hair loss can lead to serious psychological problems and have a negative impact on people's social life [1]. To this end, hair transplantation procedure has become a popular treatment for the hair loss problem. Nowadays, follicular unit extraction (FUE) and follicular unit transplantation (FUT) are the most widely accepted techniques. FUT hair transplantation refers to the process of designating a portion of the non-balding area as the donor area, cutting out a strip of scalp from this area, and then dissecting the scalp into follicular units under a microscope. These follicular units are subsequently transplanted into the balding areas [2]. On the other hand, FUE hair transplantation involves harvesting individual healthy hair follicle units directly from the non-balding region of the patient's scalp (significantly smaller in quantity compared to the size of scalp obtained through FUT technique) and then implanting them into the balding areas [3]. Compared to FUT, FUE does not leave visible scars and allows for shorter post-operative recovery [4,5]. Therefore, FUE procedure has become the most popular hair loss treatment.

The manual hair transplantation device Neograft developed by Venus Concept consists of three parts: a hair knife, a handheld pneumatic pressure device, and a sharp punch blades, as well as a handheld pneumatic graft implanter [6]. The pneumatic punching device is controlled by a foot pedal and is connected to a vacuum tube. This vacuum tube collects the grafts and keeps them stored until they are implanted into the recipient area. Based on the test by Harris [7], the extraction rate of grafts using this system is approximately 680 per hour.

The surgically advanced follicle extraction (SAFE) system developed by Harris [8,9] is also a commonly used manual hair transplantation device. This technique is divided into two methods: manual extraction and powered extraction. The former reduces follicle stripping and addresses the issue of torsion but is limited in speed. The latter, although potentially increasing the occurrence of buried grafts and having a slower extraction rate, offers the advantage of increased speed.

Conventional hair transplantation surgery uses manual devices (including hair transplanters and tweezers, etc.), and it usually involves thousands of follicle units during the transplantation surgery. Therefore, conventional hair transplantation is a highly repetitive task, and long-term manual execution of the same process is quite tedious for operators [10,11].

Modern manual hair transplantation surgery has become relatively mature and reliable, ensuring the integrity of the majority of transplanted hair follicles. However, due to the significant time and skill requirements of manual hair transplantation [7], there is a growing interest in reducing the technical barriers and

* Corresponding author.
E-mail address: wangjiaole@hit.edu.cn (J. Wang).

[1] Given his role as Managing Guest Editor of this journal, Jiaole Wang had no involvement in the peer-review of this article and had no access to information regarding its peer-review. Full responsibility for the editorial process for this article was delegated to Prof. Max Q.-H. Meng.

https://doi.org/10.1016/j.birob.2023.100128

costs, and achieving automation and improved efficiency in hair transplantation procedures [12].

Restoration Robotics is currently leading the research in the field of robotic hair transplantation. They have commercialized the ARTAS robot, which utilizes FUE technique, and have released a new version with hair implantation functionality. Compared to conventional manual devices, a handheld automatic hair implantation device is developed to reduce the frequency of device or cartridge replacement, making the hair transplantation process more continuous and shortening the operation time [12]. In 2014, the ARTAS robot achieved autonomous motion without manual assistance, continuously identifying and separating hair follicle units from surrounding tissues on the scalp [13]. However, the ARTAS system utilizes two distinct mechanical needles for both follicle extraction and implantation, resulting in a complex design that incurs high costs. Additionally, the transplantation of extracted grafts still necessitates manual intervention, preventing the realization of a fully automated procedure.

To automate the process of the follicle extraction, Zingaretti et al. have proposed an automated system for extracting hair follicles from the surface [14], which can identify the growth phase of hair to determine the follicles for extraction. This system achieves complete automation for the procedures of hair follicle extraction. In order to automate the process of the follicle implantation, Oostman has provided a device for efficient loading, storage, and replacement of hair grafts [15], which can be used for batch storage of hair follicles. It also provides an improved execution mechanism and operational method for ejecting hair grafts from the container of the support cylinder, realizing the automation of the hair transplantation process. Additionally, Oostman has proposed a structure design for a hair implantation needle but not used for follicle extraction [16]. This design allows for a smaller opening compared to traditional subcutaneous needles and facilitates the placement and retention of hair grafts when the needle is withdrawn from the body surface.

However, these efforts are limited to automating certain aspects of hair transplantation procedures or optimizing the processes of hair extraction and transplantation, and they have not achieved complete automation in the whole procedure of the hair transplantation surgery.

1.2. Contributions

In this paper, we propose an pneumatic hair transplantation mechanism and a visual-based hair transplantation strategy, with the "Sense-Extract-Implant" concept. The contributions are as follows:

(1) Design of a pneumatic hair transplantation mechanism. The transplantation mechanism can be installed on the end-effector of a manipulator, providing both extraction and implantation functions with high flexibility and adaptability. The application of airflow also enables the mechanism to transfer extracted follicles automatically.
(2) The utilization of visual feedback technology to assist hair transplantation. A camera is positioned on the mechanism at the end of the manipulator, helping to locate hair follicles by visual feedback and then solve the coordinate transformation problem in both hair implanting and extraction processes.
(3) The overall design and conduction of the experiment. Comprehensive experiments have conducted to perform follicle recognition, extraction, and implantation on a phantom of scalp with hairs.

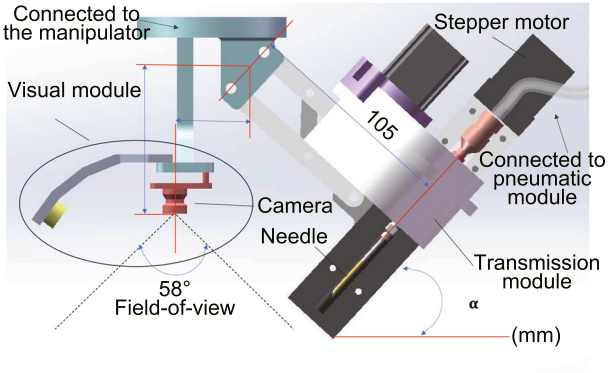

Fig. 1. The pneumatic hair transplantation mechanism (PHTM) and the dimensions of each module.

The remainder of the article is as follows. Section 2 explains the structure design of the pneumatic hair transplantation mechanism. Section 3 introduces hair transplantation strategy based on visual feedback. Section 4 presents the design of the experimental phantom and experimental process and results. Section 5 concludes the paper.

2. Design of pneumatic hair transplantation mechanism

The pneumatic hair transplantation mechanism (PHTM) proposed in this paper relies on airflow for hair extraction and hair implantation. The main mechanism is built around the pneumatic circuit for hair transplantation, which adopts the modular design method that can be divided into pneumatic module, visual module, transmission module and needle module. In this way, hair follicles are protected by airflow in the process of hair transplantation and the trauma to the scalp is also reduced. The key of the design is how to improve the overall air tightness under the premise of meeting the functional requirements. At the same time, the PHTM integrates the functions required for hair transplantation, therefore it can be mounted to a multi-DoF robotic manipulator to complete the task. The design of PHTM and the dimensions of each module are shown in Fig. 1. The top of the blue 3D printed part is connected to the end-effector of manipulator, and the lower end is equipped with the visual module. The transmission module is mounted to a lead screw which is connected to the 3D printed part through some aluminum alloy rods. The lead screw is driven by a stepper motor that drives the needle tip. The angle formed between the needle and the scalp plane is consistent with angle of hair represented by α.

2.1. Pneumatic module

Fig. 2 shows the pneumatic circuit diagram of pneumatic module. Air supply for pneumatic module adopts vacuum pump of model VN-C1 (YCZX, China) which has two interfaces, air inlet and outlet. The vacuum degree can reach −80 kPa in the aspirating state. The two interfaces of the vacuum pump are connected to a selector valve with three positions and four ways. Three positions separately lead to blowing state, aspirating state and closed state. In addition, the switch of selector valve is connected to a servo to perform automatic switching of the blowing and aspirating states. The other two ways of the selector valve are connected to the atmosphere and the pipe leading to needle, respectively.

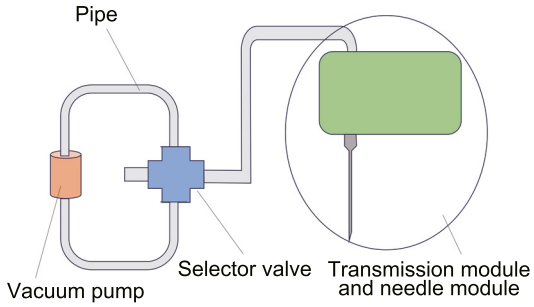

Fig. 2. The pneumatic circuit diagram of pneumatic module.

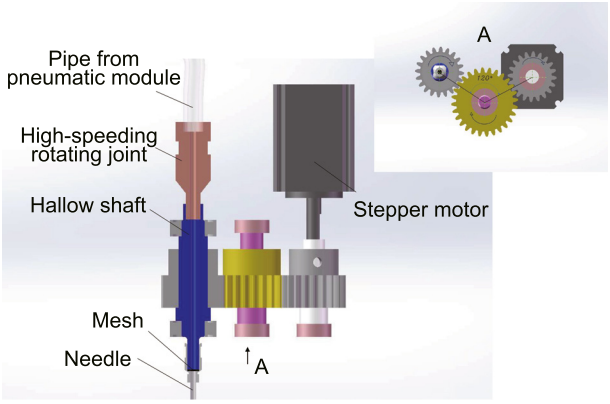

Fig. 3. Internal structure of transmission module. The transmission ratio of transmission module is 1 : 1.

2.2. Visual module

The visual module includes a camera and a light source, which are circled in Fig. 1. The visual module adopts a OpenMV4 H7 Plus camera (Singtown, China) which is located in the middle. Its field of view is about 58°. The light source (a 5 V LED point light source) is fixed on the left side of the camera to provide sufficient light for visual recognition. The light source have three mounting points which correspond to different angles of the light source. In order to obtain a clear field of view, the camera is arranged in a biased manner to ensure that the needle is away from the camera's field of view after the needle is retracted, thereby reducing the difficulty of recognition.

2.3. Transmission module

The transmission module consists of two parts. The lead screw driven by a stepper motor performs the linear motion of the needle. There is another stepper motor that performs the rotating motion of the needle, and the transmission parts are three cylindrical gears. The three gears are arranged at a certain angle to ensure that the needle can rotate without interference as shown in Fig. 3. Their modulus is 1, and the ratio of tooth number is 20:28:20. The output shaft is a hollow shaft, and the top of the hollow shaft is connected with a high-speed rotary joint to isolate the rotation of the hollow shaft. In others words, it prevents the pipe from rotating during the implantation process. The bottom of the hollow shaft is connected to the needle.

2.4. Needle module

In order to form pneumatic circuit, the needle module includes an inner needle and an outer needle as shown in Fig. 4. The inner needle is a syringe needle, and the outer needle is 0.2 mm thick aluminum sheet. The outer needle is coated on the outer wall of the inner needle by glue (Loctite 480), leaving a gap parallel to the axis for exhaust. This design prevents wound expansion or bulging caused by gas accumulation. In order to make hair follicles temporarily stored in the needle during the transportation, a mesh is set between the hollow shaft and the needle.

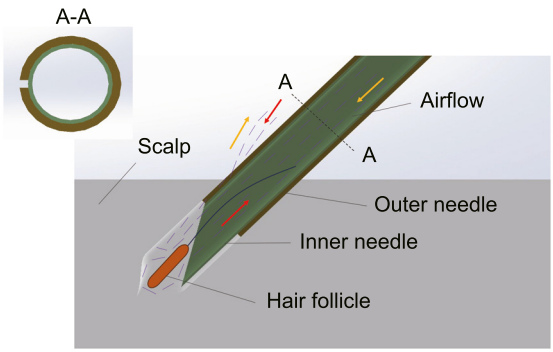

Fig. 4. The structure of the needle and the principle diagram of hair transplantation. A-A is section view of needle. The red arrow is the direction of the airflow for hair extraction, and the yellow arrow is the direction of the airflow for hair implantation.

3. Hair transplantation strategy based on visual feedback

In this section, we will first discuss how to locate hair follicles by visual feedback and then solve the visual feedback problem in both hair implanting and extraction processes.

3.1. Assumptions and conventions

In the actual robotic hair transplantation surgery, it is necessary to install a square tensioner on the scalp (Fig. 5) [17]. The tensioner can give a pressure to the scalp, and determine the transplantation area. Four corner points on the tensioner are taken as calibration points, $A_0 - A_3$ (Fig. 6), which determine the scalp frame $\{S\}$. Calibration points can be detected by a camera and then a Hough transformation on the image. Human scalp presents a spatial curved surface, but when the hair transplant area is limited to a small range inside the tensioner, it can be regarded as a plane. The relationship among camera frame $\{C\}$, manipulator's base frame $\{B\}$ and scalp frame $\{S\}$ is shown in Fig. 6.

Before the hair transplantation, the patient's hair needs to be cut short and cleaned. Therefore it can be considered that there is no overlapping between hairs, and there is no foreign body on the scalp.

In each hair extraction process and hair implantation process, considering the actual surgery inside a local area of the tensioner, every angle between the axis of hair follicle and the scalp plane are required to be a constant value. It would be best if this angle is α of PHTM, which can be easily changed according to requirement. Therefore, it is necessary to adjust z_c axis to be perpendicular to the scalp plane.

3.2. Visual-based hair extraction process

3.2.1. Camera pose adjustment

Before capturing an image of the extraction area, it is necessary to ensure that the relative pose between the camera and

Fig. 5. The tensioner used in artas robot hair transplanting surgery.

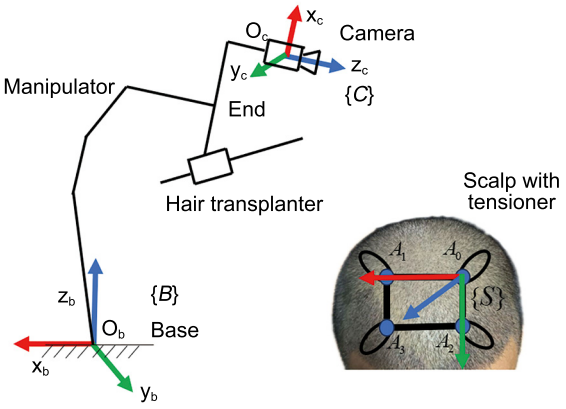

Fig. 6. The relationship among $\{C\}$, $\{B\}$ and $\{S\}$.

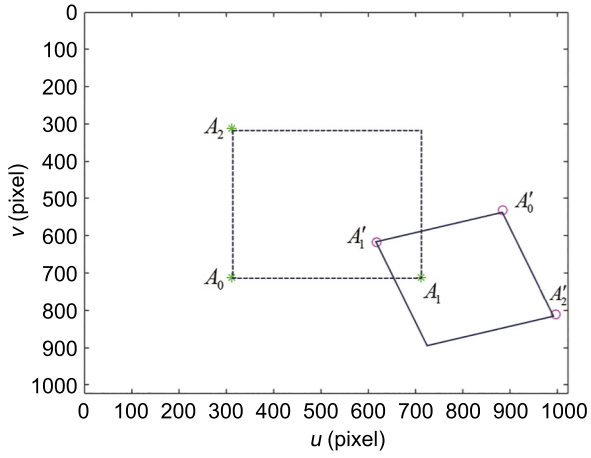

Fig. 7. An example of how to use camera to position the tensioner. $A'_0A'_1A'_2$ is the projection of the actual calibration points. $A_0A_1A_2$ is the expected position of the calibration points.

the tensioner is a preset value. This can be achieved by moving the calibration points $A_0 - A_2$ to coincide with the preset pixel coordinates (Fig. 7). This is an image-based visual servoing (IBVS) problem, and Fig. 8 is its control system.

Consider a camera moving at $v = (v_x, v_y, v_z, \omega_x, \omega_y, \omega_z)$ in $\{B\}$ and observe the spatial point $P = (X, Y, Z)$ in $\{C\}$. The velocity of

Algorithm 1: The identification of the hair extraction points.

Input: An image of an area of a scalp with some hair follicles on it: I_0
Output: A matrix of pixel coordinates of all the hair extraction points from I_0: Q

Initialize Q;
Preprocess I_0 (including converting into a gray image and Gaussian filtering), and the result is I_1;
Carry out Canny edge detection on I_1, and the result is a collection of contours: *contours*;
$n = 0$;
foreach *countour in countours* **do**
  y_{max}=0;
  foreach *i in countour* **do**
    if $y_{max} <= i[1]$ **then**
      $y_{max} = i[1]$;
      $Q[n] = i$;
    $n++$;
Output Q;

P in $\{C\}$ is

$$\begin{cases} \dot{X} = Y\omega_z - Z\omega_y - v_x \\ \dot{Y} = Z\omega_x - X\omega_z - v_y \\ \dot{Z} = X\omega_y - Y\omega_x - v_z \end{cases} \tag{1}$$

The equation of perspective projection equation is

$$\begin{bmatrix} x \\ y \end{bmatrix} = \begin{bmatrix} X \\ Y \end{bmatrix} / Z \tag{2}$$

By taking the derivative of (2) and then substitute into (1), we can have

$$\begin{bmatrix} \dot{x} \\ \dot{y} \end{bmatrix} = J \cdot v \tag{3}$$

where

$$J = \begin{bmatrix} -1/Z & 0 & x/Z & xy & -(1+x^2) & y \\ 0 & -1/Z & y/Z & 1+y^2 & -xy & -x \end{bmatrix} \tag{4}$$

The relationship between normalized image plane coordinates and pixel coordinates is

$$\begin{bmatrix} \bar{u} \\ \bar{v} \end{bmatrix} = \begin{bmatrix} f_u x \\ f_v y \end{bmatrix} \tag{5}$$

where f_u and f_v are camera internal parameters, $\bar{u}$ and $\bar{v}$ are pixel coordinates relative to the optical center.

Substitute (5) into (3), and the result is

$$\dot{p} = \begin{bmatrix} \dot{\bar{u}} \\ \dot{\bar{v}} \end{bmatrix} = J_p \cdot v \tag{6}$$

where J_p is an image Jacobian matrix of one feature point,

$$J_p = \begin{bmatrix} -\frac{f_u}{Z} & 0 & \frac{\bar{u}}{Z} & \frac{\bar{u}\bar{v}}{f_u} & -(f_u + \frac{\bar{u}^2}{f_u}) & \bar{v} \\ 0 & -\frac{f_v}{Z} & \frac{\bar{v}}{Z} & f_v + \frac{\bar{v}^2}{f_v} & \frac{\bar{u}\bar{v}}{f_v} & -\bar{u} \end{bmatrix} \tag{7}$$

When N feature points are extracted we can have the following concatenated equations:

$$\dot{p} = \begin{bmatrix} J_{p1} \\ J_{p2} \\ \vdots \\ J_{pN} \end{bmatrix} v \tag{8}$$

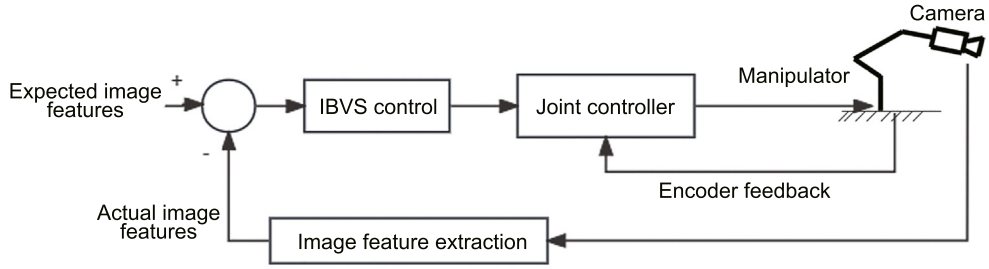

Fig. 8. IBVS control system.

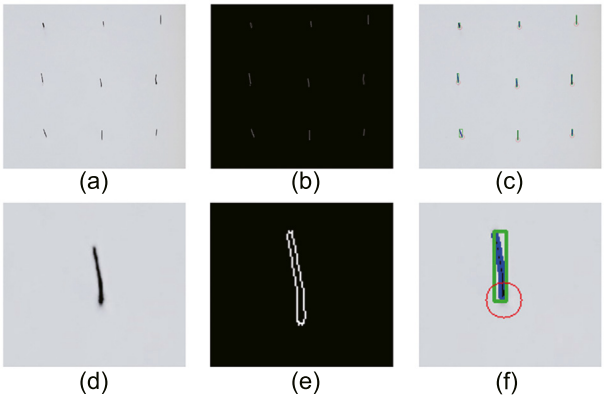

Fig. 9. The process and result of hair identification and localization. (a) is the example image with 9 hair follicles. (b) is the Canny edge detection result of (a). (c) is the result of targets in (a). (d), (e) and (f) are enlarged view of a single hair in (a), (b) and (c).

Using pseudo inverse of the Jacobian we can have

$$v = \begin{bmatrix} J_{p1} \\ J_{p2} \\ \vdots \\ J_{pN} \end{bmatrix}^{-1} \dot{p} \tag{9}$$

Eq. (9) relates the motion of the feature points to the camera motion, and it is the IBVS control equation that drives the camera, which determined the pose of the end-effector. By using the inverse kinematics of the manipulator, the corresponding joint angles can be calculated.

After camera pose adjustment, z_c axis is perpendicular to the scalp plane, and that the distance between O_c and scalp plane can be calculated as

$$h = fd/D \tag{10}$$

where f is camera focal length, D is the actual length of A_0A_1, and d is the pixel length of A_0A_1. These positional relationships will be maintained throughout the hair extraction process. h needs to be adjusted to an appropriate value for the needle tip to pierce the scalp.

3.2.2. Hair identification and localization

Taking an image of a tensioner with 9 hair follicles shown in Fig. 9(a) as an example, where all the roots of hair follicles are at the bottom of their contours, the method of locating the hair extraction points is shown in Algorithm 1.

3.2.3. Positioning of needle

When a projection of point Q_i is found on the image plane and the intersection of the needle direction and the plane is P_n, as shown in Fig. 10. To extract hair follicle at Q_i, it is necessary to ensure that Q_i and P_n coincide. Considering that the camera and hair transplantation mechanism are always relatively stationary, when the camera moves, on the image plane, point Q_i moves while point P_n remains unchanged. This can also be considered as an IBVS problem whose the control system is shown in Fig. 8. The difference is that there is only one feature point and we need to ensure that the camera only has translation on its x and y axis.

3.3. Visual-based hair implantation process

Before implanting hair, camera pose adjustment is also necessary as Fig. 7. When implanting hair, the hair follicle should be implanted at hair implanting point $P_i = (P_x, P_y)$ in $\{S\}$. We need to ensure that P_i and P_n coincide, and before that, it is easy to make A_0 and P_n coincide by IBVS method. Then, move the camera $|P_x|$ distance along the x-axis direction and $|P_y|$ distance along the negative y-axis direction to make P_i coincide with P_n.

4. Experiments and results

4.1. Experimental phantom design and fabrication

In this paper, the overall design of the experiment aims to perform follicle recognition, extraction, and implantation on a phantom of scalp with hairs. This section includes the design of the experimental phantom and experimental process and results.

4.1.1. Scalp phantom design

To simulate real hair transplantation tissue, the scalp phantom, whose upper surface is a square of 120 mm × 120 mm with a height of 15 mm, is divided into upper and lower layers [18]. The upper layer simulates the human epidermis and dermal tissues where the hair follicles are located. The surface of this region serves as the scalp plane for the experiment, with a thickness of approximately 5 mm. The lower layer simulates the subcutaneous tissue, where the subcutaneous fat is present and its main role is to cushion and support during follicle extraction and implantation process, with a thickness of approximately 10 mm.

There is a 3D-printed PLA scalp base under the scalp phantom, which simulates the skeletal structure of the human head and is connected to the experimental platform.

4.1.2. Phantom fabrication

Ecoflex 00-50 silicone gel with silicone thinner is chosen as the material for making the scalp phantom. The fabrication process involves pouring the prepared liquid silicone gel into the mold and curing to completely solidify before demolding. In this experiment, the mold (Fig. 11) is a rectangular dish with dimensions of 130 mm×130 mm×20 mm, with depth marks of 10 mm and 15 mm on the side walls. The mold is 3D printed and can be split

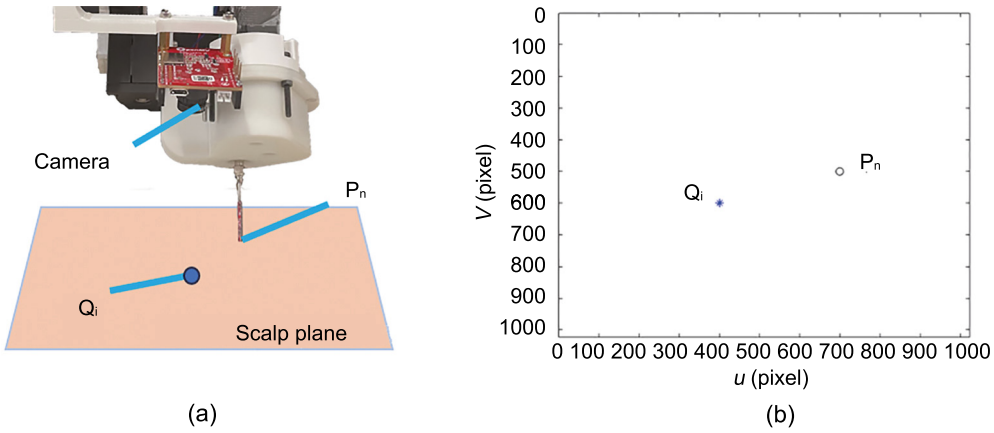

Fig. 10. Example of aligning the needle with the point. (a) reflects the relationship among Q_i, P_n and the camera. (b) shows the projections of Q_i and P_n on image plane in.

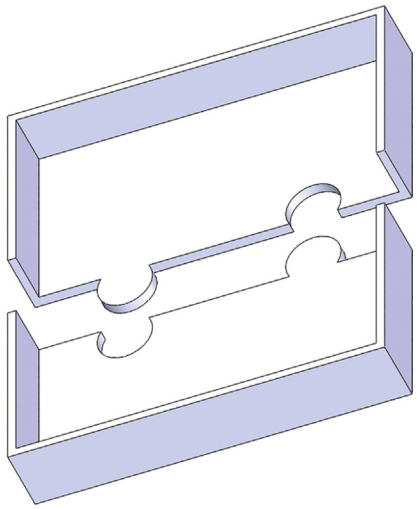

Fig. 11. Mold to fabricate the scalp phantom.

in half from the center to facilitate demolding. The steps are as follows:

(1) Preparation of the liquid silicone gel (Fig. 12). Measure equal amounts of silicone gel A and silicone gel B into a measuring cup. The function of the silicone thinner is to significantly reduce the mixing viscosity of solutions A and B, as well as lower the Shore hardness of the cured silicone gel Calculate and add the appropriate amount of silicone thinner based on the total mass of the mixed liquid, the desired hardness of the scalp model, and multiple experimental results. In this experiment, the thinner concentration for the lower layer is 5%, for the upper layer is 10%, resulting in a Shore hardness of approximately 5 A, which results in similar hardness of the human scalp [19] and can simulate the characteristic of softer epidermis and harder dermis on the scalp.

(2) Stirring and de-bubbling. Stir the mixed liquid thoroughly and use a vacuum pump to de-bubble the mixed liquid until no bubbles are generated in the cup.

(3) Pouring the scalp phantom (Fig. 13). Slowly pour the prepared lower layer liquid silicone gel into the mold up to the 10 mm mark. Let it cure for two hours, then pour the prepared upper layer liquid silicone gel into the mold up to the 15 mm mark. Let it cure for at least 24 h until completely solidified. Check for complete solidification before demolding to obtain the scalp phantom.

4.1.3. Tensioner design

The tensioner is made of 3D-printed PLA, which connects to scalp base by a tenon-and-mortise method as shown in Fig. 14. The tensioner applies pressure force to the phantom to ensure the surface to be a plane during the surgery. The center of the simulated tensioner is a square working area of 100 mm × 100 mm. There are four 4 mm calibration points on four corners of the working area, which are used as feature points in IBVS.

4.1.4. Follicle units phantom

The follicle unit phantom consists of a cylinder-shaped base, which is made of skin-colored air dry clay material, with a black pig bristle wrapped in it. Its dimensions are shown in Fig. 15.

4.1.5. Follicle chamber design

After each hair extraction and before each hair implantation, a follicle chamber is used to store hair follicles (Fig. 16). Its main part is made of 3D-printed PLA with many main holes on top of it, where the hair follicles are stored, and each main hole connects to a side hole which is connected to atmosphere. A section of PU hose, which is used to avoid air leakage and rigid collision, is embedded in the upper part of each main hole.

In the hair extraction process, the needle can be inserted into a main hole and store hair follicle as shown in Fig. 17. In the hair extraction process, with the opposite direction airflow, hair follicle can be taken out from the chamber.

4.2. Experimental process

During the hair transplantation process, the PHTM was installed on the end-effector of a 6 degree-of-freedom manipulator (ufactory xarm 6). In each hair transplantation experiment, we set $\alpha = 45°$ and $h = 60$ mm and implanted a total of 36 follicles on a 6 mm × 6 mm grid.

As shown in Fig. 18, needle depth significantly affects implanting depth during both hair implantation and hair extraction processes. While our intended implantation depth was 5 mm, after trial and error, we found that the proper needle depth was 8.5 mm, resulting in an average implantation depth of approximately 5 mm.

In the follicle implantation experiment, the manipulator, driven by the IBVS algorithm, transported each follicle from the follicle chamber and implanted them into the scalp phantom, maintaining the desired spacing and depth. Once the needle is aligned with the position to be implanted on the scalp, the stepper motor is started to guide the needle's movement until it pierces the scalp. During this process, due to the elasticity of

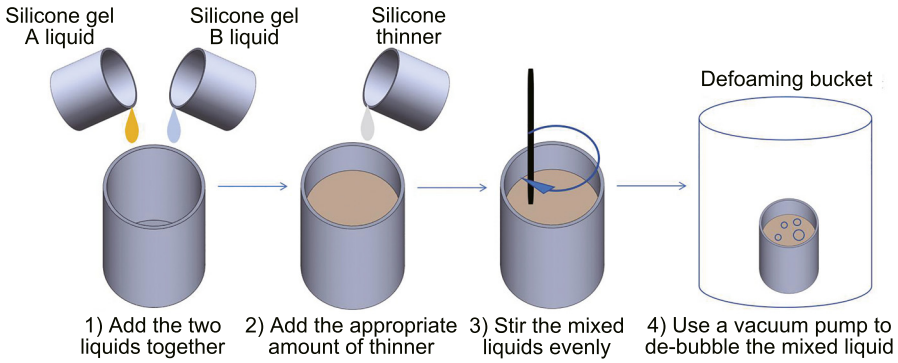

Fig. 12. Specific processes for the liquid silicone gel.

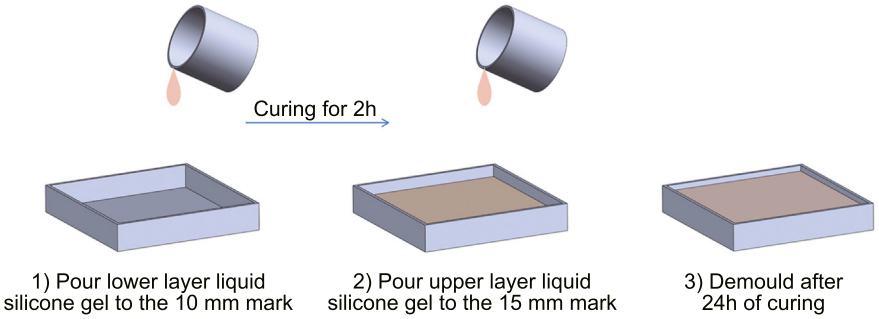

Fig. 13. Specific processes of pouring the scalp phantom.

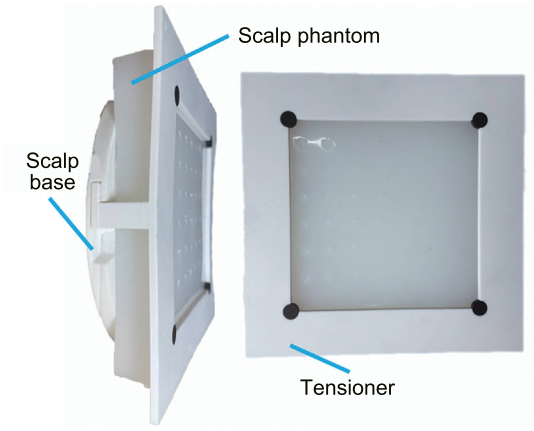

Fig. 14. The fabricated scalp phantom with the tensioner for experiments.

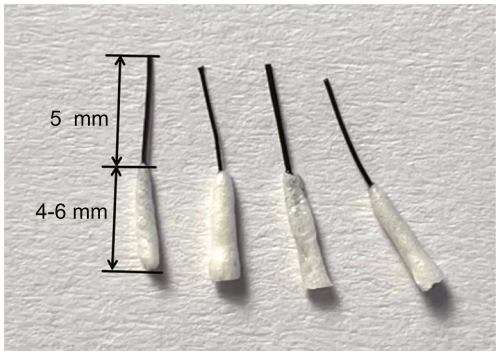

Fig. 15. Follicle units phantom. The size of the diameter of follicle part is 0.8–1.2 mm. The size of the diameter of hair is approximately 0.1 mm [20].

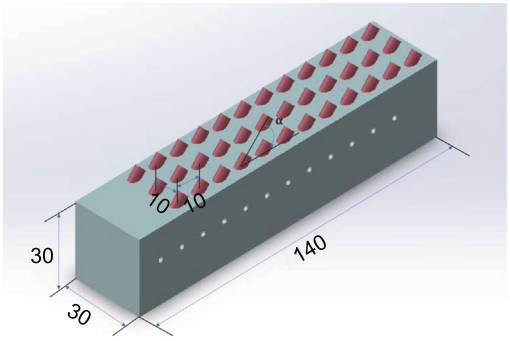

Fig. 16. The appearance and size of hair follicular chamber.

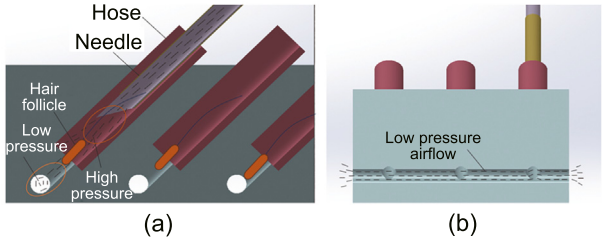

Fig. 17. Follicle chamber working principle in hair extraction process. (a) The section view of the main hole. (b) The section view of the side hole.

the scalp, the needle may not be able to fully penetrate the scalp. Therefore, the stepper motor is started to drill through the scalp after the needle has pierced the scalp. Subsequently, the selector valve is adjusted to the blowing state for hair implantation.

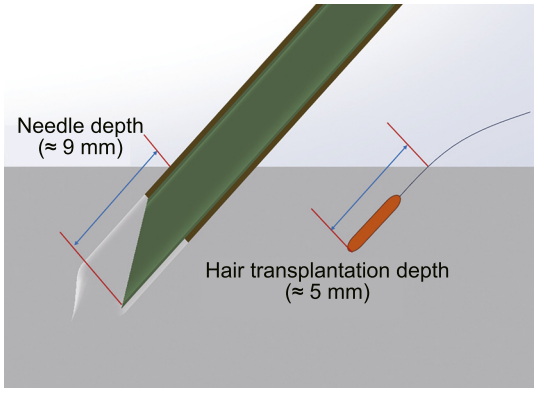

Fig. 18. The definition of needle depth and implanting depth.

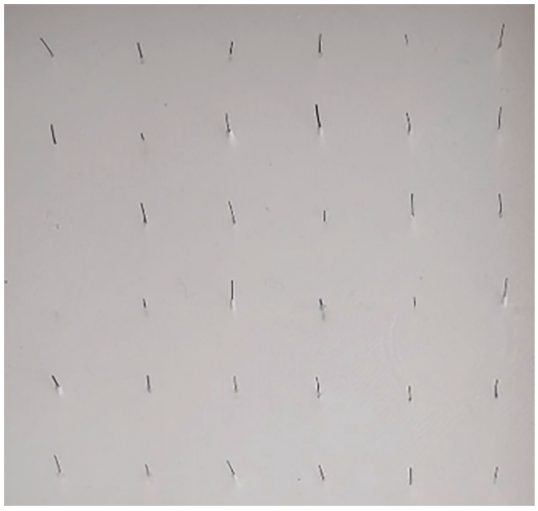

Fig. 19. Top view of a scalp phantom after an implantation experiment.

Finally, the stepper motor drives the needle to retract from the scalp in preparation for the next operation.

In the follicle extraction experiment, the manipulator extracted the previously implanted follicles from the scalp phantom and transferred them to the hair follicle chamber. Once the needle is aligned with the follicle to be extracted on the scalp, the mechanism's movement is similar to that in the implantation experiment, with the selector valve being adjusted to the aspirating state.

During follicle implantation, there were cases when follicles were not successfully implanted and were blown away by the airflow after the needle was withdrawn from the scalp phantom. These cases were considered as failed follicle implantation, where the implantation position was measured at the hole on the scalp, and the depth is measured as 0 mm. For follicle extraction, there were cases where the needle was accurately targeted at the follicle but could not successfully extract it These cases were considered as failed follicle extractions. Throughout these processes, the depth and position of each follicle and the success rate of both implantation and extraction were measured and recorded.

4.3. Experimental results

In total, three identical experiments were conducted on different scalp phantoms, and 108 sets of transplantation data were obtained. Fig. 19 is an image of the scalp phantom after a implanting experiment. It is important to note that the result of average

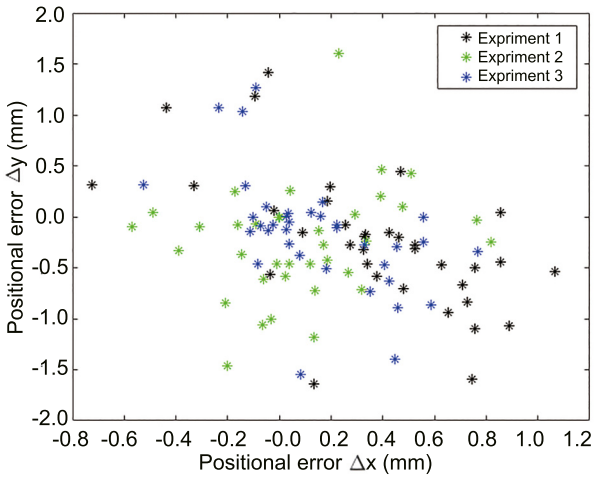

Fig. 20. The distribution of hair implantation positional errors obtained from comparing the measured positions with the desired positions.

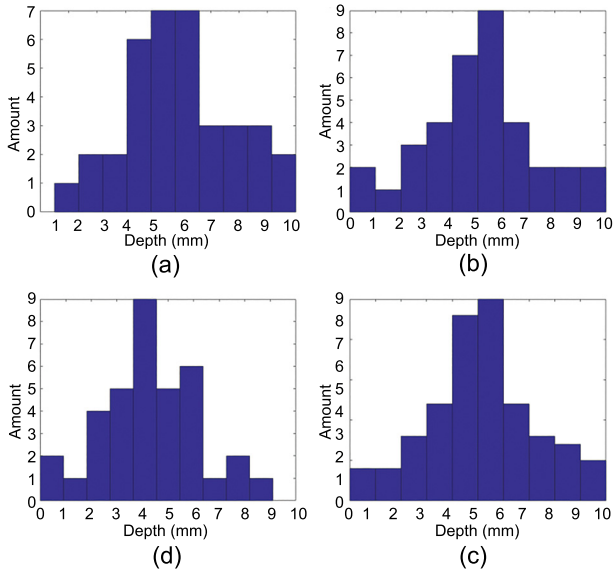

Fig. 21. Distribution of hair follicle implantation depth. (a), (b) and (c) show results of exp1, exp2 and exp3 respectively. (d) shows the total of three experiments.

positional deviation and depth deviation is much larger than the positional deviation of the manipulator, which is 0.1 mm. Thus, it can be considered that these errors mainly come from PHTM.

The distribution of relative positions are shown in Fig. 20, where both the distributions of Δx and Δy are concentrated near the origin, approximating a two-dimensional normal distribution. Table 1 presents variances and expectations concerning positional errors and deviations. Notably, the expectations for both positional errors and deviations are less than 1 mm, with relatively small variances. These findings demonstrate that the PHTM exhibits high positioning accuracy in the context of hair implantation.

The distribution of implanting depths are shown in Fig. 21, where the data from each experiment shows an approximate normal distribution. Table 2 displays the variances and expectations for both depths and depth deviations. Remarkably, the total expectation of depth (5.2269 mm) closely aligns with our anticipated depth (5.0 mm), but the expectations for deviations exceed

Table 1
Position error statistics for the hair transplantation.

Error	Exp1	Exp2	Exp3	Total
$E(\Delta x)$ (mm)	0.3521	0.0803	0.1423	0.1916
$D(\Delta x)$ (mm^2)	0.1579	0.0963	0.0759	0.1216
$E(\Delta y)$ (mm)	−0.2491	−0.2549	0.1423	−0.2218
$D(\Delta y)$ (mm^2)	0.4368	0.3017	0.3220	0.3487
$E(\Delta d$[a]$)$ (mm)	0.7575	0.5734	0.5073	0.6128
$D(\Delta d)$ (mm^2)	0.1958	0.1332	0.1809	0.1781

[a] $\Delta d = \sqrt{(\Delta x)^2 + (\Delta y)^2}$, which is positional deviation.

Table 2
Depth error of hair follicle implantation.

Error	Exp1	Exp2	Exp3	Total
$E(depth)$ (mm)	5.8972	5.4056	4.3778	5.2269
$D(depth)$ (mm^2)	4.2146	5.1651	4.2018	4.8470
$E(\Delta depth$[a]$)$ (mm)	1.6750	1.7833	1.6944	1.7176
$D(\Delta depth)$ (mm^2)	2.1568	2.0631	1.6468	1.9213

[a] $\Delta depth = |5 - depth|$, which is depth deviation.

Table 3
Success rate of implantation and extraction.

Success rate	Exp1	Exp2	Exp3	Total
Success rate of implantation	94.4%	94.4%	91.7%	93.5%
Success rate of extraction	75.0%	77.8%	77.8%	76.9%

1 mm, accompanied by a relatively large variance. These findings suggest that in the context of hair implantation, the PHTM demonstrates strong depth trueness while there is potential for enhancing its depth precision.

The success rates of implantation and extraction are shown in Table 3, where the total success rate of implantation is above 90% while the total success rate of extraction is less than 90%. Therefore, PHTM has good stability in implantation, while the stability of extraction function needs to improve.

5. Conclusion

This paper presents a pneumatic hair transplantation mechanism, which, compared to purely mechanical hair transplantation mechanism, has the ability to automatically store follicles and use only one needle to operate both hair implantation and extraction, resulting in relatively lower costs and higher automation. Furthermore, we have designed a IBVS hair transplantation and extraction method for this mechanism and conducted preliminary experimental to vertify its transplanting and extracting functions.

In the future work, we will focus on studying the process of needle penetration into the scalp at a theoretical level, aiming to further improve the success rate of transplantation and extraction and enhancing the stability of follicle implantation depth.

Declaration of competing interest

The authors declare that they have no known competing financial interests or personal relationships that could have appeared to influence the work reported in this paper.

Acknowledgments

This work was supported by Special Funds for the Cultivation of Guangdong College Students' Scientific and Technological Innovation (Pdjh2022b0568).

Appendix A. Supplementary data

Supplementary material related to this article can be found online at https://doi.org/10.1016/j.birob.2023.100128.

References

[1] R.L. Lin, L. Garibyan, A.B. Kimball, L.A. Drake, Systemic causes of hair loss, Ann. Med. 48 (6) (2016) 393–402.
[2] D.E. Rousso, P.M. Presti, Follicular unit transplantation, Facial Plast. Surg. 24 (04) (2008) 381–388.
[3] W.R. Rassman, R.M. Bernstein, R. McClellan, R. Jones, E. Worton, H. Uyttendaele, Follicular unit extraction: minimally invasive surgery for hair transplantation, Dermatol. Surg. 28 (8) (2002) 720–728.
[4] R. Sharma, A. Ranjan, Follicular unit extraction (FUE) hair transplant: curves ahead, J. Maxillofacial Oral Surg. 18 (4) (2019) 509–517.
[5] J.A. Harris, Follicular unit transplantation: dissecting and planting techniques, Facial Plast. Surg. Clin. 12 (2) (2004) 225–232.
[6] L.M. Bicknell, N. Kash, C. Kavouspour, R.M. Rashid, Follicular unit extraction hair transplant harvest: a review of current recommendations and future considerations, Dermatol. Online J. 20 (3) (2014).
[7] P.T. Rose, The latest innovations in hair transplantation, Facial Plast. Surg. 27 (04) (2011) 366–377.
[8] W.P. Unger, R. Shapiro, R. Unger, M. Unger, Hair Transplantation, CRC Press, 2010.
[9] J.A. Harris, The SAFE System®: new instrumentation and methodology to improve follicular unit extraction (FUE), in: Hair Transplant Forum International, Vol. 14, Hair Transplant Forum International, 2004, pp. 157–164.
[10] J.-w. Suh, E.-c. Choi, Design and verification of a gravity-compensated tool handler for supporting an automatic hair-implanting device, IEEE Robot. Autom. Lett. 4 (4) (2019) 4410–4417.
[11] R.M. Bernstein, Integrating robotic FUE into a hair transplant practice, in: Hair Transplant Forum Intl, Vol. 22, 2012, pp. 228–229.
[12] R.M. Bernstein, M.B. Wolfeld, Robotic follicular unit graft selection, Dermatol. Surg. 42 (6) (2016) 710–714.
[13] R.M. Rashid, Follicular unit extraction with the Artas robotic hair transplant system system: an evaluation of FUE yield, Dermatol. Online J. 20 (4) (2014).
[14] G. Zingaretti, J.W. McCollum, M. Bodduluri, P.L. Gildenberg, D.E. Caddes, Automated System and Method for Hair Removal, US Patent 10,299,871, 2019.
[15] C.A. Oostman Jr., Instruments, Systems and Methods for Improving Hair Transplantation, US Patent 9,974,565, 2018.
[16] C.A. Oostman Jr., S.E. Jakubowski, Implantation needle, US Patent 10,076,352, 2018.
[17] S. Christopher, P. Ognjen, Z. Gabriele, Robotic Hair Transplantation System with Touchscreen Interface for Controlling Movement of Tool, US Patent 10,387,021, 2019.
[18] D. Tolhurst, M. Carstens, R. Greco, D. Hurwitz, The surgical anatomy of the scalp, Plast. Reconstr. Surg. 87 (4) (1991) 603—12, discussion 613—4.
[19] N. Pittar, T. Winter, L. Falland-Cheung, D. Tong, J. Waddell, Scalp simulation–A novel approach to site-specific biomechanical modeling of the skin, J. Mech. Behav. Biomed. Mater. 77 (2018) 308–313.
[20] A. Dua, K. Dua, Follicular unit extraction hair transplant, J. Cutan. Aesthet. Surg. 3 (2) (2010) 76.